

Performance of the ISS-CREAM calorimeter in a calibration beam test

H.G. Zhang^a, D. Angelaszek^{a,b}, M. Copley^a, J.H. Han^a, H.G. Huh^a, Y.S. Hwang^{c,e}, H.J. Hyun^{c,h}, K.C. Kim^a, M.H. Kim^a, H.J. Kim^c, K. Kwashnak^a, M.H. Lee^{a,d,*}, J.P. Lundquist^a, L. Lutz^a, A. Malinin^a, H. Park^c, J.M. Park^{c,f}, N. Picot-Clemente^a, E.S. Seo^{a,b,**}, J. Smith^a, J. Wu^a, Z.Y. Yin^a, Y.S. Yoon^{a,g},

^a*Institute for Physical Science and Technology, University of Maryland, College Park, MD 20742, USA*

^b*Department of Physics, University of Maryland, College Park, MD 20742, USA*

^c*Department of Physics, Kyungpook National University, Daegu 41566, Korea*

^d*Center for Underground Physics, Institute for Basic Science (IBS), Daejeon 34126, Korea*

^e*Korea Atomic Energy Research Institute, Gyeongju 38180, Korea*

^f*Advanced Radiation Technology Institute, Korea Atomic Energy Research Institute, Jeongseup 56212, Korea*

^g*Korea Research Institute of Standards and Science, Daejeon 34113, Korea*

^h*Pohang Accelerator Laboratory, Pohang 37673, Korea*

Abstract

The Cosmic Ray Energetics And Mass experiment for the International Space Station (ISS-CREAM) was installed on the ISS to measure high-energy cosmic-ray elemental spectra for the charge range $Z = 1$ to 26. This ISS-CREAM instrument consists of a tungsten scintillating-fiber calorimeter preceded by carbon targets for energy measurements. The carbon target induces hadronic interactions so showers develop in the calorimeter. Energy deposition in the calorimeter determines the particle energy.

As a predecessor, the balloon-borne CREAM instrument was successfully flown seven times over Antarctica for a cumulative exposure of 191 days. The CREAM calorimeter demonstrated its capability to measure energies of

*Corresponding author: mhlee@ibs.re.kr

**Corresponding author: seo@umd.edu

Corresponding author: ysy@kriss.re.kr

cosmic-ray particles, and the ISS-CREAM calorimeter is expected to have a similar performance. Before the launch, an engineering-unit calorimeter was shipped to CERN for a beam test calibration. The performance test includes position, energy, and angle scans of electron and pion beams together with a high voltage scan for calibration and characterization. In addition, an attenuation effect in the scintillating fibers was measured. In this paper, beam test results including corrections for the attenuation effect are presented.

Keywords: ISS-CREAM, cosmic rays, calorimeter, calibration, energy response, attenuation

1. Introduction

The balloon-borne experiment CREAM [1] and its successor ISS-CREAM [2] were designed to directly measure the cosmic-ray elemental spectra from protons to iron nuclei, especially including electrons for the ISS-CREAM, for energies ranging from a few hundred GeV over a few PeV. The balloon-borne CREAM instrument completed seven successful operations circumnavigating Antarctica under the long duration balloon and its accumulated exposure was approximately 191 days. The CREAM instrument proved the capability to measure cosmic-ray elemental spectra over a few hundred TeV. Measured elemental energy spectra and relative abundances of primary cosmic rays nuclei were reported [3, 4, 5, 6]. A limitation of energy measurement in the CREAM experiment was caused by measurement exposure, so the CREAM instrument was transformed to be installed on the International Space Station (ISS) for more statistics and higher energy reaches.

In August 2017, the ISS-CREAM payload was launched and deployed on the ISS, and in February 2019, the ISS-CREAM instrument has finished its mission, with 546 days of data collected and to be analyzed (more details can be found in [7, 8, 9]). The detailed description of the ISS-CREAM sub-detectors are available at elsewhere [10, 11, 12, 13, 14]. Before the launch, an ISS-CREAM engineering-unit [15], a copy of the flight unit, was taken to the European Organization for Nuclear Research (CERN) and exposed to electron and pion beams for calorimeter calibration and performance tests of the instrument. In this paper, we report the analysis results of the calibration test and performance of the calorimeter.

2. Instrument

The basic design of the calorimeter for the CREAM and the ISS-CREAM experiments are the same, as shown in Fig. 1. A calorimeter unit consists of carbon targets and a calorimeter. In order to make the detector comply with space-launch requirements, the calorimeter was modified to accommodate the mechanical strengths due to transportation. More details would be available on the ISS-CREAM instrument references.

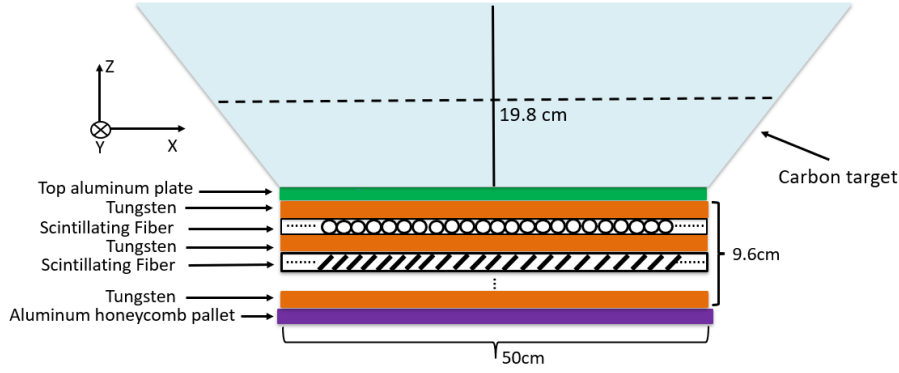


Figure 1. A sectional view of the calorimeter and the carbon target. The calorimeter is composed of 20-layers of tungsten plates and 1000 scintillating fiber ribbons between layers (not to scale).

The calorimeter unit initiates the hadronic showers upstream of the calorimeter with two light blocks of densified graphite with a density of 1.92 g/cm^3 and a total thickness of 19.75 cm as a target, which corresponds to one radiation length and 0.5 nuclear interaction length. A significant portion of the electromagnetic shower core and the shower maximum in the longitudinal shower profile is contained in the tungsten/scintillating fiber ribbon layers, which produces a high energy trigger in the calorimeter. Fig. 1 shows a cross-sectional view in $[X, Z]$ plane of the calorimeter stack on top of an aluminum honeycomb pallet with a total height of 9.5 cm , preceded by the densified-graphite target.

There placed twenty $3.5\text{-mm-thick } 50\text{cm} \times 50\text{cm}$ tungsten plates below the target, which serve as the passive medium. Each tungsten plate corresponds to one radiation lengths. Between each of two consecutive tungsten layers, a layer with fifty fiber ribbons is placed and covering the same area covered

by the tungsten plate. While half of the fiber ribbons, which are every other ribbon, are mated with light guides on one side of the calorimeter, the other half are mated on the opposite side. The dimensions of the fiber ribbon are $1\text{ cm} \times 50\text{ cm}$ with an effective thickness of 0.64 mm including glue to combine nineteen fibers.

On each ribbon with nineteen 0.5-mm-diameter scintillating fibers, the scintillation lights generated by charged particles in the shower are transmitted to a hybrid photodiode (HPD) via a light mixer and a bundle of clear fibers [10]. The light signal is divided into three different sub-bundles, low, mid, and high ranges by different numbers of clear fibers (42, 5, and 1 respectively). Combining the three optical sub-ranges gives enough dynamic range to cover energies of the measured cosmic-ray particles. After the conversion of the photons as photo-electrons in the photo-cathode of the HPDs, the photo-electrons accelerated between the photo-cathode and a pixelated silicon diode create electron-hole pairs. The pairs are read out by a charge amplifier and then sent to both a fast-shaping circuit for a trigger and a slow-shaping circuit to be digitized with an analog to digital converter (ADC) chip (more details can be found in [16]).

3. Calorimeter calibration

The purpose of the calorimeter calibration is to obtain a calibration factor to convert a raw ADC signal to value in the energy unit, MeV, for each ribbon. An initial calibration factor can be estimated by a ratio of deposits in Monte Carlo simulation to beam response of each ribbon. Additional correction factors for the calibration factor can be added by iterative processes such as attenuation correction or gain correction, if necessary.

For the initial calibration factor estimation, the response of each ribbon was measured with electron beams along Z direction by shifting beam position along with X or Y direction. We used an electron beam of 150 GeV with a beam profile in a Gaussian distribution of $\sim 4.6\text{-mm}$ σ from the beam trigger counter ($2\text{ cm} \times 2\text{ cm}$) to calibrate the readout channels of the fiber ribbons. As shown in Fig. 2, a position with ribbons numbered 22 (the 22nd ribbons from -X or -Y side) of odd layers in the calorimeter were exposed to beams. Then, after collecting enough data, the calorimeter was moved by 1 cm along -Y direction to place the next ribbon center exposed to the beams. Position adjustment and measurement were repeated for all fifty ribbons in

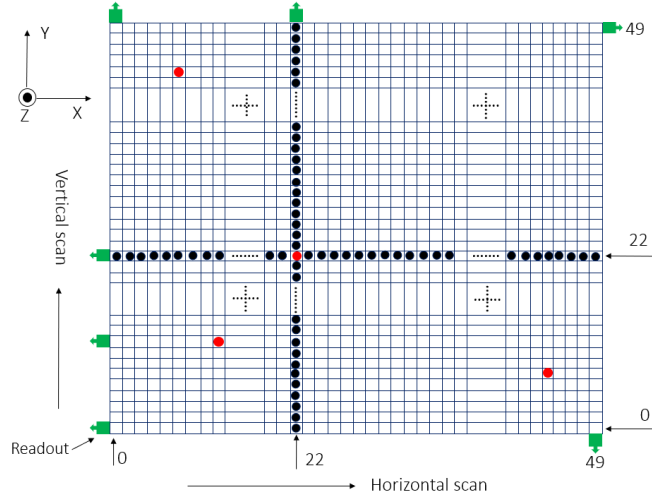


Figure 2. Part of the first two-layers of the calorimeter ribbon layout, and the **beam hit-position** illustration. Layer with ribbons aligned along $\pm Y$ **direction** are **exposed to beams with a hit-position** by moving along $\pm X$ -direction, while the other layers with ribbons aligned $\pm X$ **direction** are **exposed to beams with a hit-position** by moving along $\pm Y$ direction. The black filled circles represent the incident electron beam spots, while the red filled circles are considered for a position uniformity study in section 5.5.

the odd layers. In the same way, the calorimeter was moved by 1 cm along $-X$ direction to place all the ribbon centers of even layers to the beams, as well.

The four detector configurations were implemented to measure response of ribbons throughout the calorimeter. We calibrate the ribbons in the top four layers and the bottom four layers using measurements in “Lead-Front” and “Lead-Rear” configurations, respectively, and we calibrate ribbons in layers 5-10 and 11-16 with measurements in “No-Lead-Front” and “No-Lead-Rear” configurations, respectively.

In the “No-Lead-Front” configuration, the electron beam was injected in front of the graphite target to get a detector response from the electron shower particles passing through ribbons in the middle layers. The “No-Lead-Rear” configuration is similar, however, the electron beam was then injected with the instrument rotated by **180 degree** so that the electron beam was incident on the bottom. **As you can see in Fig. 4, top layers and bottom layers have relatively small intensity of signals in**

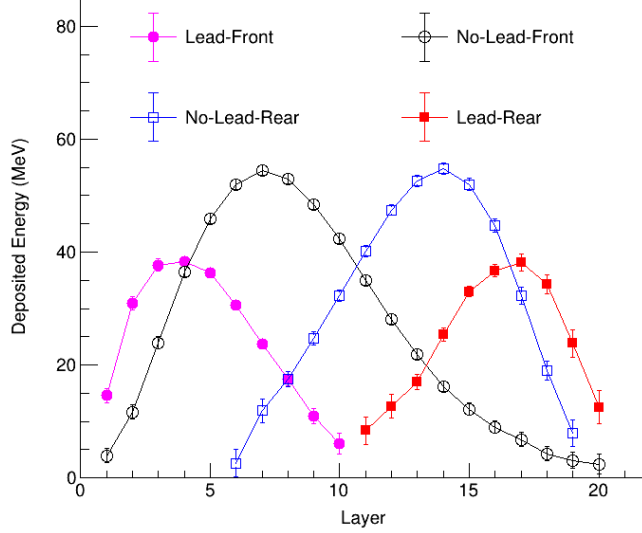


Figure 3. Deposited energy on fiber ribbon from Monte Carlo (MC) simulation results using 150 GeV electron beams. We perform four detector configurations in the beam line, “Lead-Front”(filled circles), “No-Lead-Front”(open squares), “No-Lead-Rear”(open circles), and “Lead-Rear”(filled squares), in order to place shower maximum positions from top to bottom of the calorimeter evenly.

the “No-Lead-Front” and “No-Lead-Rear” configurations. To have larger intensity of signals at top and bottom layers, lead bricks were positioned before the calorimeter unit. In the “Lead-Front” configuration, 2.5-cm-thick lead bricks were placed in front of the graphite target to place the shower maximum in the first few layers where the showers have not been initiated in previous two configurations. The “Lead-Rear” configuration is similar, however, the lead bricks were placed when instrument rotated to calibrate the bottom layers. Also, two tungsten plates were placed between the honeycomb pallet and the lead bricks to compensate for the two missing radiation lengths of the carbon target. The Monte Carlo (MC) simulations were performed with the four configurations as well and results with an equalization process are shown in Fig. 3.

Although the incident beam spot is known for the fiber ribbon number and physical position, particles in the shower can hit the neighboring fiber ribbons, because not only the shower has lateral shower profile but also the

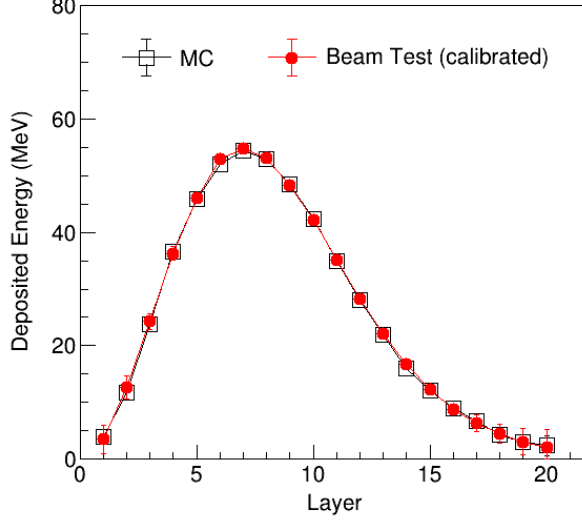


Figure 4. The comparison of deposited energy in each layer (150 GeV electron) from calibrated data (filled circles) with that from MC simulation (open squares).

beam width is wider than the width of a ribbon width, 1cm. Only those events at which the fiber ribbon nominally in the beam and records the maximum are selected in the analysis of MC results and beam measurement data. To select the appropriate events, we also implemented a pre-selection cut to subtract the hadronic events from the contaminated hadron particles (i.e., pions).

As shown in Fig. 4, the deposited energies from the calibrated data agree perfectly with those from the simulation results. The linearity of the calorimeter response were confirmed with the CREAM calorimeter using fragmented heavy-ion beams at CERN [17]. It should be applied to the ISS-CREAM calorimeter as well, since the design of the ISS-CREAM calorimeter was the same to the CREAM calorimeter. In addition, MC simulation results of the CREAM and ISS-CREAM calorimeter indicate that a calorimeter response is quite linear in the measurement energy range [18, 19].

4. The attenuation effect and the energy response

When a ribbon position where beams hit is changed from 0 to 49 along with -X or -Y direction, a ribbon laying orthogonal direction to moving direc-

tion, which is on the targeting layer, is changed as well according to ribbon position. However, a ribbon laying parallel to the moving direction, which is above or below the targeting layer, did not change, when the beam position is changed. On the same ribbon above or below the targeting layer, data were collected at 50 positions with every 1cm distance from the one end to the other end. The attenuation effect was studied using ribbons laying parallel to the moving direction in beam scan data.

As scintillation lights pass through a fiber ribbon, they interact with the material and getting weaker, and the intensity decreases exponentially with the distance to the readout $\Delta(x)$ in a form of $e^{-\Delta(x)/\lambda}$, where λ is the attenuation length.

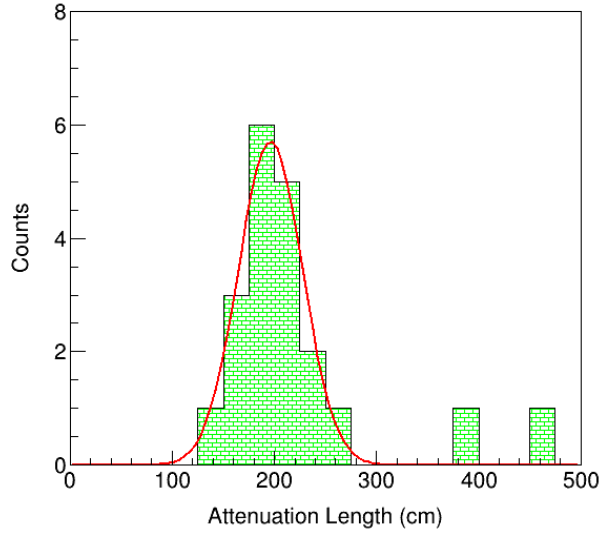


Figure 5. The distribution of attenuation lengths of twenty ribbons from 20 layers, and it is fitted by a Gaussian function.

As shown in Fig. 5, the distribution of the attenuation length values for different ribbons at beam ribbon in 20 layers shows a Gaussian distribution, and the most probable value of the attenuation length is found to be 196cm (the mean value is fitted to be 196 cm while the σ is fitted to be 31.4), which implies the intensity of the signal drops to around 80% when it passes through the whole ribbon length of 50 cm. In addition to that, because the attenuation length values of twenty different ribbons are given in a Gaussian

distribution, it can be assumed the rest ribbons have the same trend. In this paper, we applied this most probable attenuation length to all the 1000 ribbons in the calorimeter.

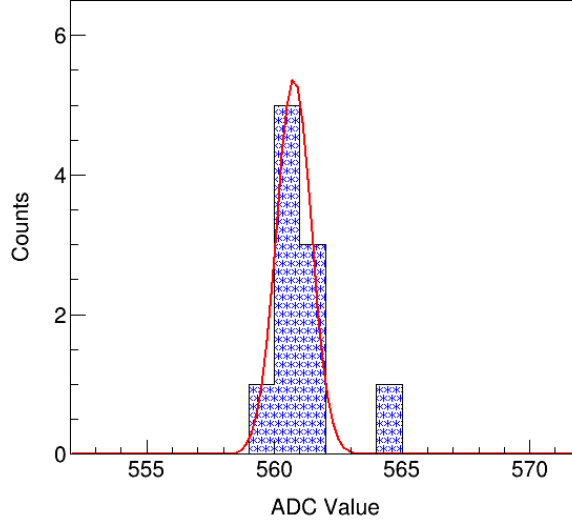


Figure 6. Distribution of the signal response (and its Gaussian fitting) on ribbon 22 in layer 8 with 10-times repeated measurements at $[22, 22]$ in $[X, Y]$ plane, and it is fitted by a Gaussian function.

The variation of signal responses at each position is carefully checked in this work, and it shows good stability. As illustrated in Fig. 6, the distribution of the responses with 10 repeated measurements at the crossing point $[22, 22]$ in layer 8, shows a narrow Gaussian distribution. The mean value at this point to be found at 561, and the σ is found to be small (0.68), which implies a good stability of the measured ADC value.

We correct the attenuation effect of the deposited energy at each point in this work, and after that we study the energy response of primary particle by summing over all of the deposited energies on ribbons that are exposing to the shower in section 5.

5. The energy response and resolution

We use the electron energy scan, the pion energy scan, the angle scan, and the high voltage scan to characterize the energy responses of the calorimeter.

The result is reported in this section. In section 5.5, we explain how the energy responses changed by the attenuation corrections, and in section 5.6, we check if the energy of the primary particle has fully deposited in the calorimeter.

The incident beam position is fixed at $[8, 8]$ in $[X, Y]$ plane for electron energy scan and pion energy scan, while for angle scan and high voltage scan, the incident position is fixed at $[36, 36]$ in $[X, Y]$ plane.

5.1. Electron energy response measurements

The responses of ribbons were measured with electron beams with energies varying from 50GeV to 175GeV to characterize the energy response of the calorimeter, and we performed a pre-selection with a cut on the sum of five neighboring fiber ribbons and layers to remove the hadronic events.

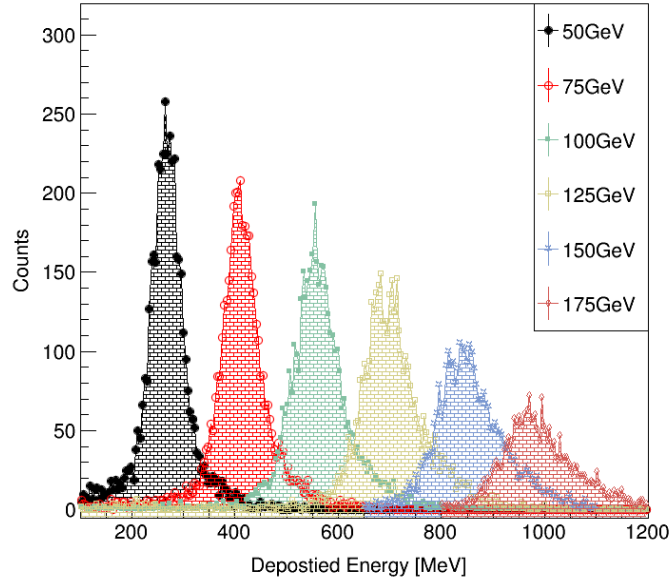


Figure 7. Calorimeter responses of energy deposits from incident electron beam energies of 50, 75, 100, 125, 150, and 175 GeV, which are distinguished by symbols and colors. The attenuation correction has been considered.

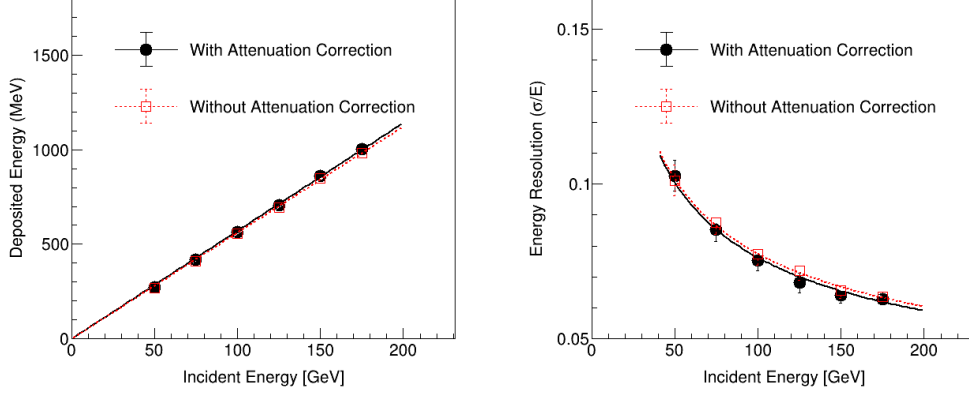


Figure 8. Mean energy deposit in the calorimeter as a function of the incident electron beam energies (left). Energy resolution of the calorimeter as a function of the incident electron beam energies (right). We compare the cases with attenuation correction (filled circles with black solid line) and without attenuation correction (open squares with red dashed line).

The deposited energy distributions from various incident energy electron beams are shown in Fig. 7. Gaussian function fits are used to determine the mean energy deposits in the detector. The energy response of the calorimeter as shown in Fig. 8 (left) proves to be linear with increasing incident electron beam energies, with a slope of 5.70 MeV/GeV, and the deposited energy with 150 GeV incident beam is found to be 850 MeV. For the case without the attenuation correction, the slope is found to be 5.65 MeV/GeV, which is consistent with that of balloon-borne CREAM calorimeter at previous beam tests (see [15]).

As shown in Fig. 8 (right), the energy resolution with respect to the incident electron beam energy is fitted by using the quadratic function with a constant term, $\sigma_E/E = 0.59/\sqrt{E(\text{GeV})} \oplus 0.02$ when considering the attenuation correction. The energy resolution is found to be 10.0% at 50 GeV and improves with increasing energy, reaching 6.60% at 150 GeV. The smaller (higher) energy resolution at higher energy is due to more number of shower particles generated in the calorimeter compared with that for low energy electrons. For the case without attenuation correction, the energy resolution is found to be $\sigma_E/E = 0.58/\sqrt{E(\text{GeV})} \oplus 0.02$, and at 150 GeV, the resolution is 6.65%.

5.2. Pion energy response measurements

The calorimeter aims to measure the electromagnetic component of hadronic showers induced in the preceding carbon target by high-energy interacting nuclei. The responses of ribbons were measured with pion beams with energies from 250 GeV to 350 GeV to characterize the energy response of the calorimeter to incident hadrons.

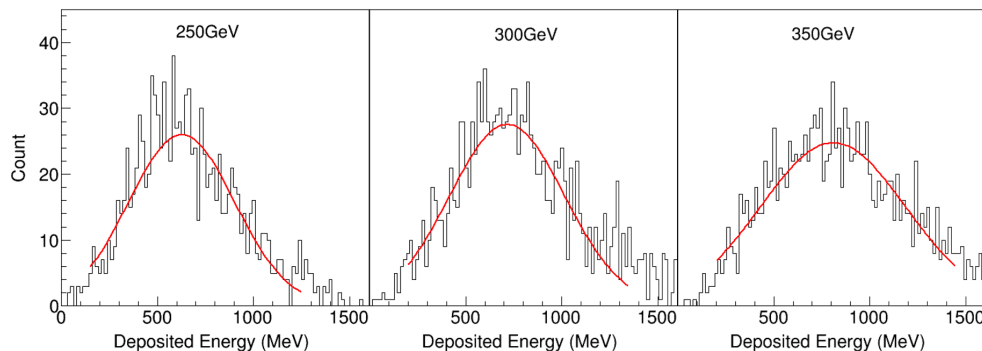


Figure 9. Energy deposits in calorimeter for pion beams with incident energies of 250 GeV (left), 300 GeV (middle), and 350 GeV (right). The distributions are fitted by Gaussian functions.

To obtain only pion events that interacted in the carbon target upstream of the calorimeter, we performed a pre-selection cut requiring events with enough signals in the first three layers of the calorimeter, to obtain a good Gaussian distribution. The deposited energies with summing over five ribbons and layers at the center on the beam position with incident energies of 250 GeV, 300 GeV, and 350 GeV are shown in Fig. 9.

As shown in Fig. 10 (left), the dependence of the deposited energy to the incident energy of the pion beam is observed to be linear. After applying the attenuation correction, the slope is found to be 1.9 MeV/GeV, which is $1/3$ of the electron beam. This is consistent with theoretical expectations that when cosmic-ray particles (mainly protons) interacting hadronically with the calorimeter, on average approximately $1/3$ of the energy of the primary nuclei is converted into neutral pion π^0 , which then rapidly decay into two photons with the electromagnetic showers produced [9]. For the case without attenuation correction, the slope is found to be 1.92 MeV/GeV, which agrees with the fraction of balloon-borne CREAM calorimeter (see [20]).

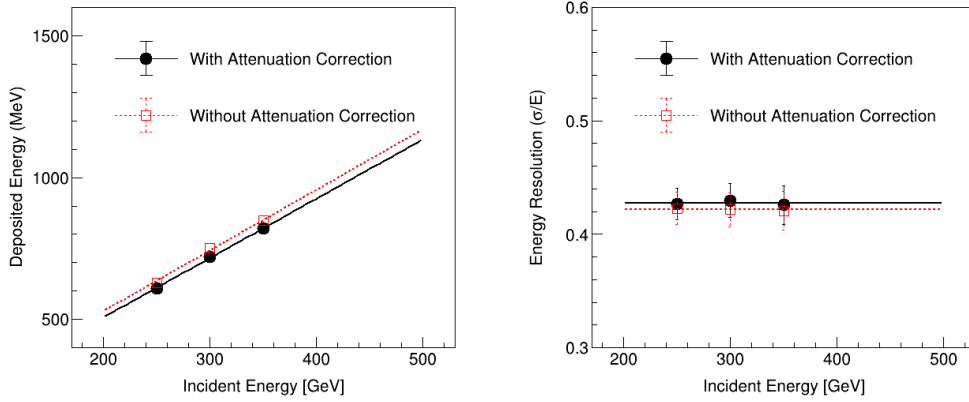


Figure 10. Mean energy deposit in the calorimeter (left) and energy resolution of the calorimeter (right) as a function of the incident pion beam energy. We compare the cases with attenuation correction (filled circles with black solid line) and without attenuation correction (open squares with red dashed line).

As shown in Fig. 10 (right), the energy resolution is found to be 42.7%, which is independent of incident energy, while for the case without attenuation correction, the energy resolution is found to be 42.2%.

5.3. Electron angle response measurements

The incident cosmic-ray particles to the detector from various angles in space show good isotropic approximation. We did an angle scan to characterize the angular response of the calorimeter. Measurement of the electron beam at a fixed energy of 150 GeV was performed with three different incident beam angles of 0° , 30° , and 45° .

The ADC response of ribbons for angle scan is shown in Fig. 11 in -X direction. The pattern represents the electromagnetic shower from an electron beam with an energy of 150 GeV at an incident angle of 30° . We see the electrons traverse the whole detector and produce showers with energy deposited in each layer.

After applying the attenuation correction, in Fig. 12 (left), we illustrated a function of deposited energy with increasing incident energy by fitting with a linear function with a slope of $1.57 \text{ MeV}/^\circ$ (the fitting function is $1.57 \times A + 854$ where A is the angle), approximately 70 MeV increases from 0° to 45° , which could be from containing more shower particles in the later part of longitudinal shower development by having more effective absorber

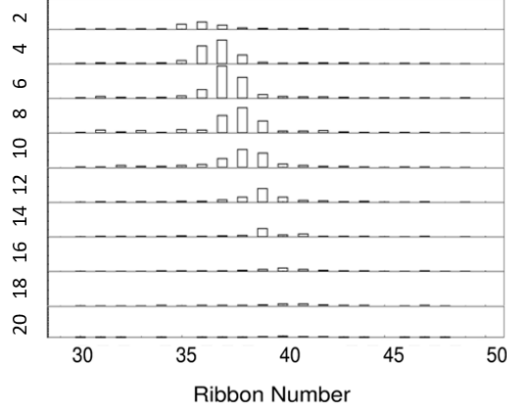


Figure 11. An event display example of ADC response of ribbons in -X direction (even layers) using 150 GeV electron beam with incident angle of 30° . The height of the rectangle represents the ADC value of each ribbon.

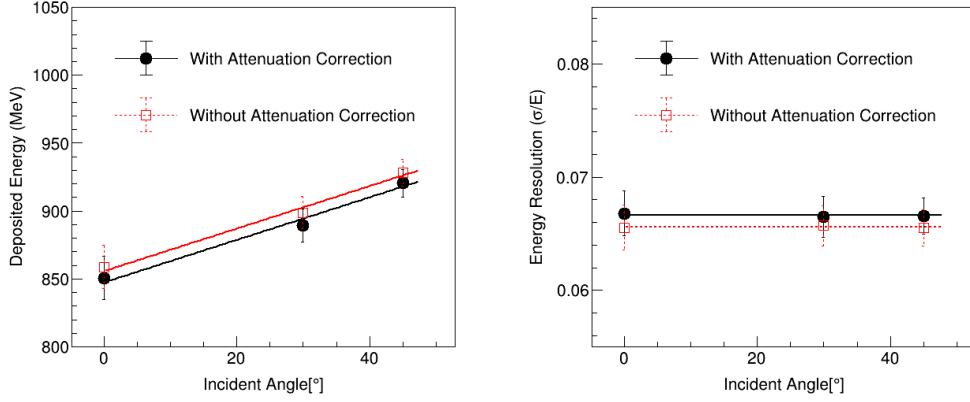


Figure 12. Mean energy deposit in the calorimeter (left) and energy resolution (right) as a function of the incident angles using 150 GeV electron beam. We compare the cases with attenuation correction (filled circles with black solid line) and without attenuation correction (open squares with red dashed line).

thickness. The deposited energy at 0° is found to be 854 MeV which is consistent with what we observed in section 5.1. While without attenuation correction, we find the energy response with increasing incident energy is fitted by $1.58 \times A + 845$.

The deviation of deposited energy with 45° for 150 GeV electrons is ap-

proximately 8.3%. The deviation by angles at the energy of TeV can be estimated using Monte Carlo simulations since test beams with energy over TeV are not available for detector calibration. While for the case without attenuation correction, the resolution is approximately 6.65%, which is consistent with the energy scan result in section 5.1.

5.4. Measurements with different high voltage settings

The calorimeter energy response with respect to the applied high voltage (HV) of the HPD is studied in this section. This test was necessary for calibration of a calorimeter on a balloon-borne CREAM experiment, which used different HV setting vales on the HPD during the flight at the altitude of ~ 40 km, compared to those set at the beam calibration, to avoid damages from corona discharges. For the calorimeter on the ISS-CREAM, the HV setting values of the HPD are the same values to the calibration test on the ground. However, the HV scan test was performed in case of any possible situation with different HV setting values in the flight.

We used the HV gain correction in the range of [4 kV, 10.5 kV] to reconstruct the deposited energy of flight data. The ADC sum with respect to the HPD high voltage was tested at a fixed incident electron beam energy of 150 GeV by changing the HV setting values.

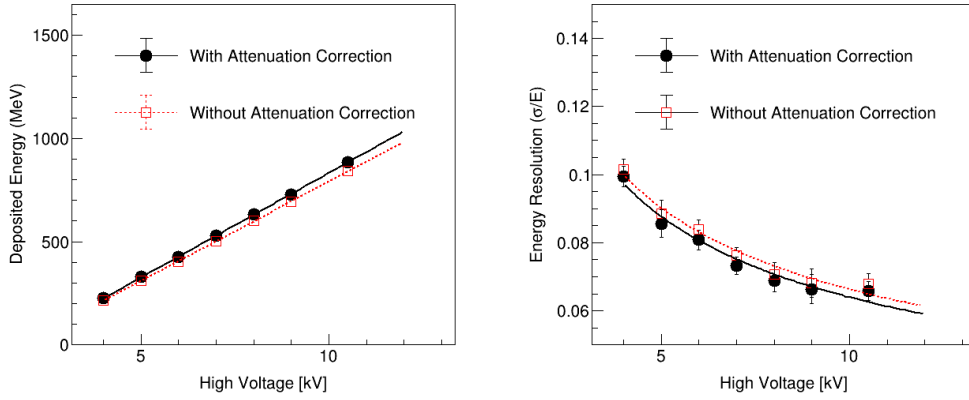


Figure 13. Mean energy deposit in the calorimeter (left) and energy resolution of the calorimeter (right) as a function of the high voltages using 150 GeV electron beam. We compare the cases with attenuation correction (filled circles with black solid line) and without attenuation correction (open squares with red dashed line).

After applying the attenuation correction, we show in Fig. 13 (left) that the deposited energy as a function of high voltage is fitted by a linear function with a slope of 101 MeV/kV(the fitting function is $101 \times \text{HV} - 180.0$). The deposited energy is fitted to be 850 MeV for 10.5 kV, which is consistent with what was shown in section 5.1. For the case without attenuation correction, deposited energy as a function of high voltage is fitted by $96.5 \times \text{HV} - 172.5$.

As shown in Fig. 13, the energy resolution of calorimeter for electron beam as a function of HV is fitted using the quadratic function $\sigma_E/E(H) = 0.188/\sqrt{\text{HV}(\text{kV})} \oplus 0.01$. We observe that the energy resolution at 10.5 kV is approximately 6.6%, which is consistent with the resolution(6.4%) obtained in section 5.1, where the voltage is 10.5 kV, too. For the case without attenuation correction, the energy resolution is fitted by the function $\sigma_E/E(H) = 0.185/\sqrt{H(\text{kV})} \oplus 0.01$, and the value at 10.5 kV is 6.70% which is consistent with what we found in section 5.1 (6.60%).

5.5. Analysis of the attenuation correction

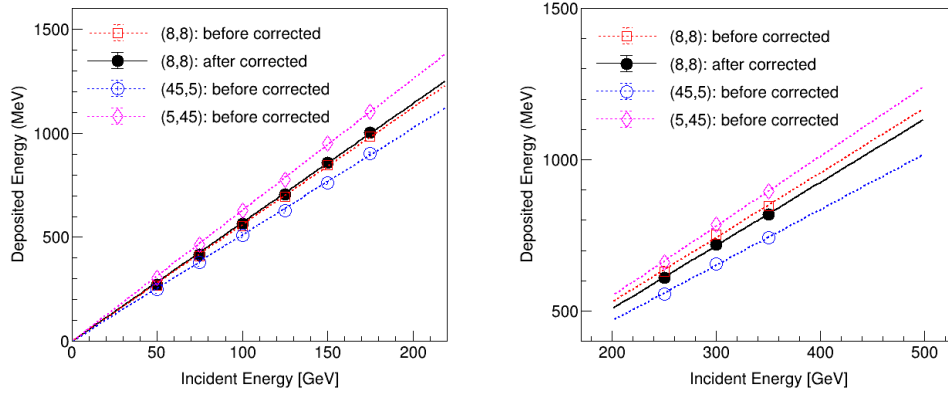


Figure 14. The comparison of the energy responses before attenuation effect correction at [8,8](open squares), [45,5](open circles) and [5,45](open diamonds), with the energy response after attenuation correction at [8,8](filled circles). Left). The case for electron beam. Right). The case for pion beam.

We compare the energy responses (at [8,8], [45,5] and [5,45]) before attenuation effect correction with that after correction in Fig. 14. We show the responses for electron beam and pion beam, and we find for both cases, the energy responses before attenuation at [45,5] and [5,45] are about 10%

higher and 10% lower than the response after attenuation correction. This gives us an example of how the energy responses changed by the attenuation correction at different positions.

5.6. Longitudinal shower profile in the calorimeter

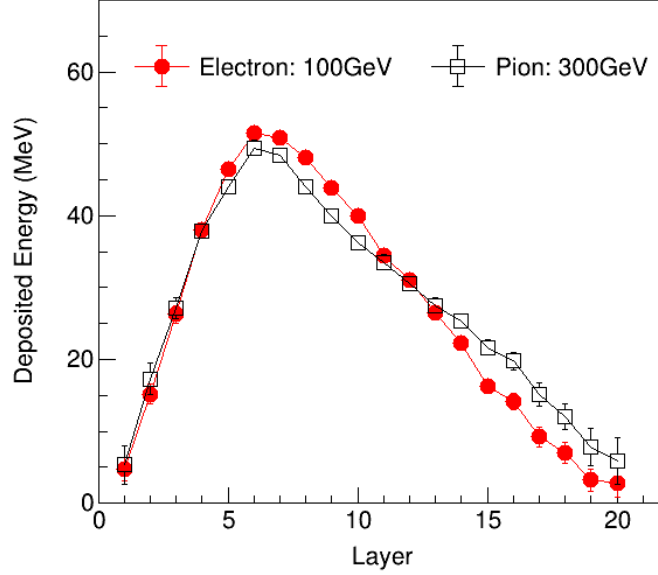


Figure 15. The energy deposit in the calorimeter summing over five ribbons in each layer for electron beams (filled circles) and pion beams (open squares). We measured the deposited energy from the calibrated data with 10-times repeated beam test at $[8, 8]$ in $[X, Y]$ plane after the attenuation correction has been applied.

As the sampling fraction of the pion beam is approximately $1/3$ of the electron beam, the deposited energies from 100 GeV electron beam and 300 GeV pion beam are similar. We show the longitudinal shower profiles of 100 GeV electron beam and 300 GeV pion beam in Fig. 15 with respect to layer number by summing over the neighboring five ribbons. We see the shower from the pion beam is wider than that from the electron beam. But for both cases, the primary particles have fully converted their energies into scintillation light, which implies the linearity we find in sections 5.1 and 5.2 is solid.

6. Conclusion

The ISS-CREAM detector is designed to measure the energies of the cosmic-ray particles with energies over a few hundred GeV. To characterize its performance, an engineering-unit calorimeter was calibrated at CERN using electron and pion beams before its launch.

The energy responses to both electron and pion beams are generated with attenuation effect corrected. The performance of the ISS-CREAM detector was found to be comparable to previous CREAM calorimeters. Analysis shows the distributions of deposited energy for both electron beam and pion beam are Gaussian. The energy responses prove to be linear with increasing incident beam energies for electron and pion beams. For electron beam, the slope is found to be 5.70 MeV/GeV, and the energy resolution is approaching to 6.60% at 150 GeV. For pion beam, the slope is found to be 1.9 MeV/GeV, and the resolution, which is independent of the incident energy, is found to be 42.7%. The result of this paper will be used for flight data analysis.

7. Acknowledgments

This work was supported in the U.S. by NASA grant NNX17AB41G, in Korea by National Research Foundation grants 2018R1A2A1A05022685 and 2018R1A6A1A06024970, and their predecessor grants. It was also supported in France by IN2P3/CNRS and CNES and in Mexico by DGAPA-UNAM project IN109617. The authors also thank the support of CERN for the excellent beam test facilities and operations. The authors thank NASA GSFC WFF and its contractors for engineering support and project management, JSC ISS Program Office for the launch support and ISS accommodation, MSFC for the operational support, and KSC and SpaceX for the launch support.

References

- [1] E. Seo et al., Cosmic-ray energetics and mass (CREAM) balloon project, *Adv. Space Res.* 33 (10) (2004) 1777.
- [2] E. Seo et al., Cosmic Ray Energetics And Mass for the InternationalSpace Station (ISS-CREAM), *Adv. Space Res.* 53 (10) (2014) 1451.
- [3] H. Ahn et al., Discrepant hardening observed in cosmic-ray elemental-spectra, *ApJL* 714 (2010) L89.

- [4] Y. Yoon et al., Proton and Helium Spectra from the CREAM-III Flight, *ApJ* 839 (1) (2017) 5.
- [5] H. S. Ahn et al., Energy spectra of cosmic-ray nuclei at high energies, *The Astrophysical Journal* 707 (1) (2009) 593603. doi:10.1088/0004-637x/707/1/593.
- [6] H. S. Ahn et al., Measurements of the relative abundances of high-energy cosmic-ray nuclei in the TeV/nucleon region, *ApJ* 715 (2) (2010) 1400.
- [7] E. Seo et al., Cosmic Ray Energetics And Mass for the International Space Station (ISS-CREAM), *PoS (ICRC2019)* 358 (2019) 137.
- [8] S. Kang et al., On-orbit performance of the top and bottom counting detectors for the ISS-CREAM experiment on the international space station, *Adv. Space Res.* 64 (12) (2019) 2564.
- [9] G. H. Choi et al., On-Orbit Performance of the ISS-CREAM SCD, *PoS(ICRC2019)* 358 (2019) 048.
- [10] I. Park et al., Silicon charge detector for the CREAM experiment, *Nucl. Instrum. Meth. A* 570 (2) (2007) 286.
- [11] J. Lee et al., The ISS-CREAM Silicon Charge Detector for identification of the charge of cosmic rays up to $z = 26$: Design, fabrication and ground-test performance, *Astropart. Phys.* 112 (2019) 8.
- [12] Y. Hwang et al., Construction and testing of a Top Counting Detector and a Bottom Counting Detector for the Cosmic Ray Energetics And Mass experiment on the International Space Station, *J. Instrum.* 10 (07) (2015) P07018.
- [13] Y. Amare et al., The boronated scintillator detector of the ISS-CREAM experiment, *Nucl. Instrum. Meth. A* 943 (2019) 162413.
- [14] H. Hyun et al., Performances of photodiode detectors for top and bottom counting detectors of ISS-CREAM experiment, *Nucl. Instrum. Meth. A* 787 (2015) 134.

- [15] J. R. Smith et al., The Cosmic Ray Energetics And Mass for the In-ternational Space Station (ISS-CREAM) Instrument, PoS (ICRC2017)301 (2018) 199.
- [16] H. Ahn et al., The cosmic ray energetics and mass (CREAM) instrument, Nucl. Instrum. Meth. A 579 (3) (2007) 1034.
- [17] H. Ahn et al., Performance of CREAM calorimeter: Results of beamtests, Nucl. Phys. B, Proc. Suppl. 150 (2006) 272.
- [18] H. Ahn et al., Cosmic Ray Energetics And Mass : Expected Performance, Proceedings of the 27th International Cosmic-Ray Conference,Hamburg 6 (2001) 2159.
- [19] J. Wu et al., Monte Carlo Simulations of the ISS-CREAM Instrument,PoS (ICRC2019) 358 (2019) 154.
- [20] J. Hahn et al., Calibration of the CREAM calorimeter with beam testdata, Proceedings of the 32nd International Cosmic-Ray Conference,Beijing 6 (2011) 399.
- [21] M. Tanabashi et al., Review of particle properties, Phys. Rev. D 98(2018) 030001.